IEEE Access
Multidisciplinary | Rapid Review | Open Access Journal

Received January 1, 2021, accepted January 13, 2021, date of publication January 22, 2021, date of current version January 29, 2021.

Digital Object Identifier 10.1109/ACCESS.2021.3053767

Estimation of Moisture Content in Thickened Tailings Dams: Machine Learning Techniques Applied to Remote Sensing Images

GABRIEL VILLAVICENCIO ARANCIBIA[1], OSVALDO PIÑA BUSTAMANTE[2], GABRIEL HERMOSILLA VIGNEAU[2], HÉCTOR ALLENDE-CID[3], GONZALO SUAZO FUENTELABA[4], AND VICTOR ARAYA NIETO[4]

[1]Escuela de Ingeniería en Construcción, Pontificia Universidad Católica de Valparaíso, Valparaiso 2147, Chile
[2]Escuela de Ingeniería Eléctrica, Pontificia Universidad Católica de Valparaíso, Valparaíso 2147, Chile
[3]Escuela de Ingeniería Informática, Pontificia Universidad Católica de Valparaíso, Valparaíso 2241, Chile
[4]Departamento de Obras Civiles, Universidad Técnica Federico Santa María, Valparaíso 1680, Chile

Corresponding author: Gabriel Villavicencio (gabriel.villavicencio@pucv.cl)

This work was supported by Pontificia Universidad Catolica de Valparaiso under Grant 37.0 / 2017.

ABSTRACT Chile is one of the major producers of copper in the world, and as such is responsible for 1.7 million tons of tailings per day. While the most commonly used deposit to store this type of mining waste is historically tailings sand dams, the mining industry has over the last two decades been inclined toward thickened tailings dams (TTD) because of their advantages in water resource recovery, lower environmental impact, and better physical and chemical stability over conventional deposits. Within the geotechnical area, one key requirement of TDD, is the need to monitor moisture content (w%) during operation, which is today mostly performed in situ – via conventional geotechnical or simple visual means by TTD operators – or off site, via remote sensing. In this work, an intelligent system is proposed that allows estimation of different classes of in-situ states and w% in TTD using Machine learning algorithms based on Artificial Neural Networks (ANN), Support Vector Machine (SVM) and Random Forest (RF). The results show an accuracy of between 94% and 97% in the classification task of the Dry, Semisolid, Plastic and Saturated classes, and between 0.356 and 0.378 of the MAE metric in the regression task, which is sufficient to estimate the w% with ML methods.

INDEX TERMS Thickened Tailings Dams, Physical Stability, Artificial Neural Networks, Remote Sensing

I. INTRODUCTION

While the Chilean mining industry produced 5600 MT of copper in 2019 – one of the major sources worldwide [1] – it is expected to reach 7.04 million tons of copper by 2030, peaking in 2027 at 7.33 million tons [2]. However, this increase in copper production implies a peak of 1.7 million tons of tailings per day which will need to be stored in surface deposits, indeed, 90% of which are predicted to need to remain active nationwide through the end of the period to meet this need.

The latest cadastre of mining operations carried out in Chile identified a total of 757 tailings deposits, with 14.7% active; 22.9%, abandoned; 61.7%, inactive; and 0.7%, in construction [3]. Historically, the most widely used tailings storage technology has been tailings dams [3]. However, these may suffer physical instability, especially in countries with significant seismic activity like Chile [4].

The high risks of great environmental and economic losses resulting from catastrophic failures of tailings deposits [4] – not to mention the imperative for greater water recovery, decreased environmental impact, and improved physical stability – have encouraged the mining industry to seek other solutions. The trend has been toward thickened tailings dams (TTD) technology, with clear advantages and benefits as a high-solid disposal and material desaturation process [5]–[7].

Nevertheless, the implementation of TTDs in Chile requires accounting for certain conditions not present elsewhere, such as scaling to much greater storage volumes, the lack of appropriately flat topography or necessary surface area, the high seismicity, and extreme meteorological events – not to mention the expected gaps in the design and operation for these types of deposits [8].

The associate editor coordinating the review of this manuscript and approving it for publication was Thomas Canhao Xu.

These factors clearly necessitate that operational control for TTDs be adequate, permanent, and high-standard. Indeed, for proper physical and chemical stability, the ideal would be affordable, continuous, geotechnical, geometric and water controls during both operational and post-closure phases. It is here that permanent operational geotechnical measurements, along with supervision and periodic inspections, play a fundamental role in the physical stability of a TTD.

One of the most important geotechnical variables to be monitored during TTD operational phases is in-situ w%. There is a practical empirical standard of tailings engineers that each deposited layer of thickened tailings should be allowed to dry until in-situ w% is equal to or less than its Shrinkage Limit (SL). This, among other benefits - such as increased density of tailings deposited on the surface by natural desiccation and the associated contraction of the tailings mass – reduces the risk of liquefaction and/or significant deformation of the TTD during seismic events [9], and is a practical criterion in planning tailings disposal sequences (discharge zones). However, like other geotechnical variables, in-situ w% exhibits great spatial and temporal variability [10], making continuous monitoring a necessity for modern mining operations.

Within this context, one of the most widely adopted monitoring strategies has become remote sensing. The advantages of this technology over conventional on-site monitoring techniques (on-site surveys, sampling, and testing) include more frequent data gathering for larger areas (100 to 1000 ha approximately) and those with difficult access. Furthermore, satellite image analysis is increasingly becoming a technology at scale in the follow-up and monitoring of tailings deposits, particularly for the control of growth, deformations, and movement of the clear water lagoon.

To this end, in reporting on combinations of remote sensing methodology, [5]–[7] evaluated the use of satellite and hyperspectral images (captured by unmanned aerial vehicle UAV) in correlating the reflection of light on the surface of a TTD and its surface w% as determined from field and laboratory tests. The results obtained in terms of the intensity of reflection normalized to dry soil was shown to have high correlation, suggesting a precise and cost-efficient technology for monitoring surface moisture in TTDs [6]. However, such approaches have yet to be extensively implemented in monitoring tailings water content. Indeed, that same study discusses how this technology may be significant in safe disposal and storage of thickened tailings, with the caveat, however, that procedures must be developed to continuously cover larger areas. A promising alternative toward building on the proposal, then, is the use of Machine Learning (ML) algorithms. Greatly advanced in recent years, ML techniques – which have been employed in solving various civil engineering problems [11] for at least 30 years – are an empirical approach for computer programs to learn from a large data set and capture functional relationships among variables, even if the fundamental relationships are unknown or their physical meaning is difficult to explain [12]. As such, ML is ideal for modeling the complex behavior of most geotechnical parameters – which by their nature are spatially and temporally variable – especially as applied to remote and continuous monitoring of w% over time in TTDs. The great modeling capacity and ability to learn from experience has catapulted ML techniques over classical approaches (e.g., statistical methods, geostatistics, among others); moreover, their application does not require hypotheses or criteria selection in addressing a particular problem [13].

The contribution of our work is twofold: Firstly, we propose a novel approach used to estimate in situ w% in TTD using Remote Sensing images. The approach, to the best of our knowledge, has never been applied to this type of task in TTDs. Secondly, we estimate an in situ variable from remote sensing images using Artificial Neural Networks (ANN), Support Vector Machine (SVM) and Random Forest (RF). Although this has been previously addressed, we demonstrate a thorough experimentation to estimate both classification and regression labels for this problem. This methodology benefits operations with continuous data monitoring, better defined TTD storage zones and growth, which will better ensure physical stability under static and dynamic conditions.

Thus the present article explores the use of the ML in monitoring w% in TTD as described above. This document is structured as follows: Section 2 presents the state of the art in the operation of TTDs and ML applied to the estimation of geotechnical variables from remote sensing images; Section 3 presents the proposed model and dataset used for the estimation of in situ w% based on satellite images; Section 4 shows the results; and the last section presents the conclusions and delineates future work.

II. STATE OF THE ART

A. OPERATION OF TTDS

To ensure physical and chemical stability – not only during operation, but also in the long term, i.e. post closure – TTDs require geotechnical, geometric, and water-related variable monitoring. These measurements identify deviations from project as designed, and, as such, potential risks related to the environment and communities located downstream.

In relation to physical stability, the control of geotechnical variables is meant to avoid scenarios that could lead to the various failure modes, e.g., seismically induced liquefaction or overtopping the retaining wall perimeter [14]. Geotechnical measurements must include: **i)** geometry of the deposit (area, height, and slope of earth structures); **ii)** physical and in situ state characteristics of the deposited tailings (percentage of solids by total weight, particle size distribution, unit weight and w%); **iii)** water table; and **iv)** specific variables carried out in the reservoir or the ground (accelerographs, settlement cells, inclinometers, among others).

Additionally, different deposition stages in TTDs require other permanent aspects for monitoring, e.g., layer thickness, plasticity of the tailings fine fraction, and drying time. As previously mentioned, surface moisture is usually considered

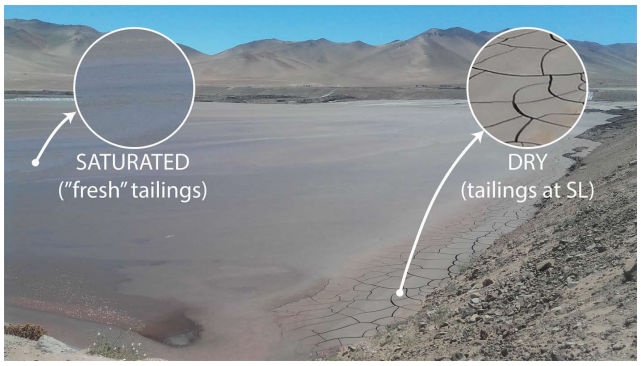

FIGURE 1. Thickened tailings deposit (TTD) in drying process.

upon disposal. This is commonly determined by visual inspection and depends on the experience of TTD operators, when the material reaches a w% equivalent to SL. Before continuing with the deposition process, the fresh tailings must lose moisture until cracks appear on the surface (Figure 1). The widths of these cracks vary from a few millimeters to 50 mm, depending on the size and mineralogy of the tailings particles [15].

Very large surface areas (from 1 to 3 ha) may be monitored with discrete surface and depth samples using boreholes. However laborious and limited to accessibility, in situ densities and tests have mostly trended toward the portable PANDA penetrometer (Pénétromètre Autonome Numérique Dynamique) in Chile [16]. This test determines tip resistance (qd) that, in the case of thickened tailings, correlate w%, the liquidity index (LI), and the field saturation condition as a function of depth [8].

Given the importance of drying time and physical stability in operating TTDs, the surface w% must be regularly monitored. Compared to the methodologies used at present, satellite images are an attractive prospecting technique for TTD monitoring.

B. MONITORING MOISTURE CONTENT BY LIGHT REFLECTION

The techniques for estimating soil moisture based on light reflection were initially developed by [17] for the control of w% in agricultural soil. That study, which carried out several tests with a spectrometer to determine the light reflection levels of a set of ten soils – composed of different proportions of clay, silt, sand, organic material, CaCO3, and Fe over a wide range of w% (from dry to saturated) – obtained a series of reflection curves as a function of w% using 12 wavelengths in the solar domain range (400 - 2500nm). After normalizing results to the reflection from dry soil condition, the obtained curves showed a parabolic relationship between light reflection and w%. Similarly, and also in the field of agricultural engineering, light reflection has been used to assess the state of crops [18]. To this end, the Normalized Difference Vegetation Index (NDVI) (1) [19] – a reflection index of combined spectral bands correlated with w% – was shown to relate light reflection with material saturation states, and thus, can be used as a valid indicator of crop health.

$$NDVI = \frac{NIR - Red}{NIR + Red} \tag{1}$$

Another soil reflection study [20] in the context of hydrology used a standardized reflection index and found a high correlation between the Short-Wave Infrared (SWIR) spectral light range (1000 - 2500nm) and surface w%. [21] expanded that index to an algorithm for use with optical satellite images and obtained a good fit in estimating surface humidity for soils, regardless of the resolution of the images.

In the context of extractive industries, [22] carried out a series of tests on oil sand tailings and found similar relationships between soil water content and light reflection as those found by [17] for soils. Furthermore, an investigation into soil w% using series of spectral images in laboratory and field conditions at light wavelengths in the solar domain (400 and 2,500nm) using a conventional Visible (VIS) camera and a Near-infrared (NIR) camera [5], [6] [7] found a high correlation between surface water content (w%) for tailings material and active illumination at 980nm, the advantages of which (lighting at a narrow spectral band) includes the ability to illuminate areas unreachable by ambient light (e.g., among the cracks generated by shrinking tailings).

The advances made in this cost-efficient, attractive methodology to estimate surface w% from light reflection have shown that spectra of in situ TTD surface moisture depends on the properties of the tailings themselves (e.g., color, particle size distribution, specific gravity of the solid phase). Thus, while experimental data from the field may still required for laboratory calibrations, techniques to extrapolate w% from at times difficult, costly, or untimely to obtain soil specimens – as well as beyond a limited, single-band spectral data, are needed. Therefore, this work presents ML techniques as a potential multidimensional image analysis alternative to more efficiently discern surface soil moisture calibrated to the needs of the current and future Chilean mining industry.

C. ARTIFICIAL INTELLIGENCE IN GEOTECHNICAL ENGINEERING

The application of Artificial Intelligence (AI) to geotechnical engineering has progressed since the 90s, and has explored techniques such as ANN, Linear Regression (LR) Analysis, Support Vector Machine (SVM), Random Forest (RF) and M5 model trees (M5P) [13], [23]–[25]. Among these AI techniques, the ANN (e.g., Multi-Layer Perceptron, MLP) have provided the best results in solving geotechnical engineering problems like modeling spatial variability of soils, estimating the overconsolidation ratio (OCR) in cohesive soils, estimating pile support capacity, estimating settlements in surface foundations, evaluating sand liquefaction susceptibility, analyzing slope stability, and predicting compaction parameters in cohesive soils, among others [24], [26].

Recent research has studied the application of AI in tailings deposits, such as: i) development of pre-alarm systems for

tailings deposits, based on real-time monitoring and numerical simulation using IoT (Internet of things) and cloud computing [27]; ii) detection of tailings deposits and mining pits from satellite images, using deep learning techniques (Deep Learning, DL) [28], [29]; iii) identification of tailings deposits using convolutional neural networks (CNNs) from satellite images and data from the registry of deposits in Brazil [30]; iv) and in identifying and monitoring surface erosion in tailings deposits using UAV images and ML [31].

In [32], the performances of ANN in retrieving soil w% and surface roughness were tested for several inversion cases (both with and without a priori knowledge of soil parameters for training). That study then validated the inversion approach using polarimetric RADARSAT-2 images. The introduction of expert knowledge was shown to improve estimates of soil w% (dry to wet soils, or very wet soils), whereas the precision on the surface roughness estimation remained unchanged. Moreover, polarimetric parameters and anisotropy improved soil parameter estimates.

There are some research works that deal with the estimation of w% using remote sensing imagery and ML methods. For example, in [33], the authors propose a novel Satellite Image Collaborated Reconstruction algorithm (SICR) in conjunction with an in situ sensor which uses an ANN to project soil w% from complex and highly variable relationships. With historical data for training, feedforward neural networks (FNNs) were shown to project in situ w% from remote sensing at better performances than conventional models. Consequently, regional moisture soil observations can be reconstructed under full cloud cover or under a total absence of sensors placed on-site. In [34] the authors proposed a machine-learning-based method to enhance spatial accuracy and improve the availability of w% data. Four ML algorithms, including classification and regression trees (CART), K-nearest neighbors (KNN), Bayesian (BAYE), and Random Forests (RF), were implemented. During the regression, the land surface temperature (including daytime temperature, nighttime temperature, and diurnal fluctuation temperature), NDVI, surface reflections (red, blue, NIR, and MIR bands), and digital elevation models were taken as explanatory variables to produce fine spatial resolution w%. The reconstructed w% datasets were validated against in situ measurements, and shown to downscale the monthly European Space Agency Climate Change Initiative (ESA CCI) w% product from 25-km to 1-km spatial resolution.

III. EXPERIMENTAL TTD AND IMAGE PROCESSING

A. GENERAL CHARACTERISTICS OF EXPERIMENTAL TTD

Located in Chile, the TTD used as an experimental field in this study corresponds to a facility that will store several millions of tons of copper tailings. The facility is located in a sector with a flat topography (3% slope on average) and characterized by a stratigraphic profile with adequate geotechnical characteristics (founded on coarse grained soils). The construction of this TTD was carried out in three deposition stages, forming ''cones'' of 5 to 10m in maximum height at the final operation stage. Tailings are discharged as a ''slurry'', forming beach slopes ranging from 2 to 7%. After tailings disposal, sedimentation, and consolidation, the drying process begins which dictates the disposal strategy, i.e. once the tailings have reached the SL, a new layer is accreted, increasing the effective overburden stress and increasing saturation of the previously disposed layer. Some design parameters of the experimental TTD are as follows: Tailing materials: sandy silts; specific gravity of the solid phase (G): 2.9; SL: 22 - 33%; targeted solid concentration at discharge of 80 to 85%; and dry unit weight at SL: 17 to 18 kN/m^3.

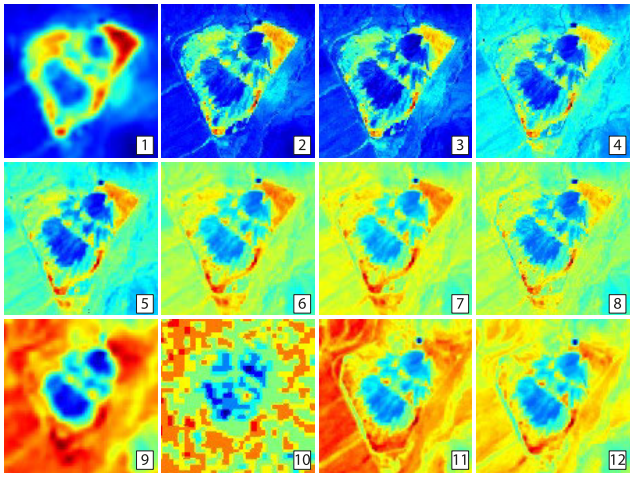

FIGURE 2. Spectral bands for the experimental TTD. October 21, 2018.

B. IMAGE PROCESSING

Image processing estimation of in situ surface w% at the experimental TTD was based on images captured over different ranges of the electromagnetic spectrum. To obtain the w%, TTD analysis used information from the visible range and the infrared spectrum to generate visible and NIR images.

Satellite images were accessed from the Sentinel 2 mission – two twin satellites (S2A and S2B) which have operated since June 23, 2015, traveling through each orbit at the same time, but out of phase by 180° – whose multispectral sensors (MSI) divides light into different bands (VNIR, SWIR). The data provides 13 spectral bands with resolutions from 10 m to 60 m. Figure 2 shows 12 of the spectral bands for the experimental TTD, corresponding to October 21, 2018 (calibration week). Spectral bands are defined as:
Band 1: Aerosols (0.43 - 0,45μm), Band 2: Blue (0.45 - 0,52μm), Band 3: Green (0.54 - 0.57μm), Band 4: Red (0.65 - 0.68μm), Band 5: Red edge 1 (0.69 - 0.71μm), Band 6: Red edge 2 (0.73 - 0.74μm), Band 7: Red edge 3 (0.77 - 0.79μm), Band 8: NIR (0.78 - 0.90μm), Band 8A: NIR (0.85 - 0.87μm), Band 9: Water vapor (0.93 - 0.95μm), Band 10: Cirrus (1.36 - 1.39μm), Band 11: SWIR 1 (1.56 - 1.65μm) and Band 12: SWIR 2 (2.10 - 2.28μm).

Combining bands 2 (blue), 3 (green), and 4 (red) reconstructs a visible image (RGB) of the TTD, in which we have highlighted different areas based on w% of the material,

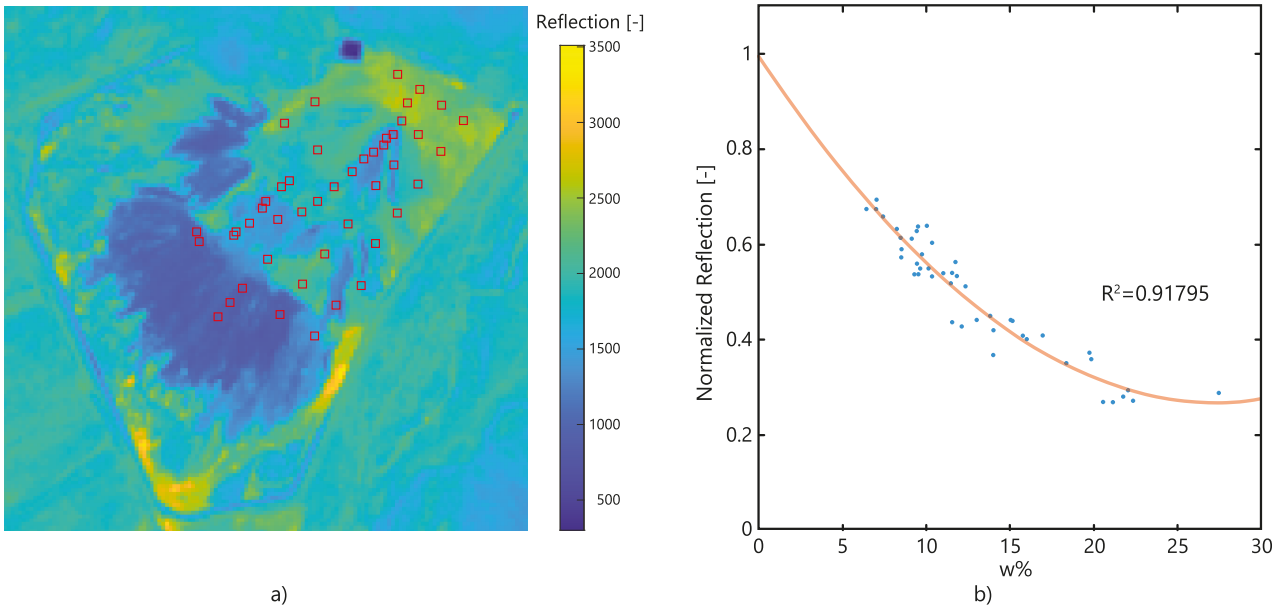

FIGURE 3. a) Light reflection in the satellite NIR band - b) Correlation between NIR band and in-situ w% obtained in the field.

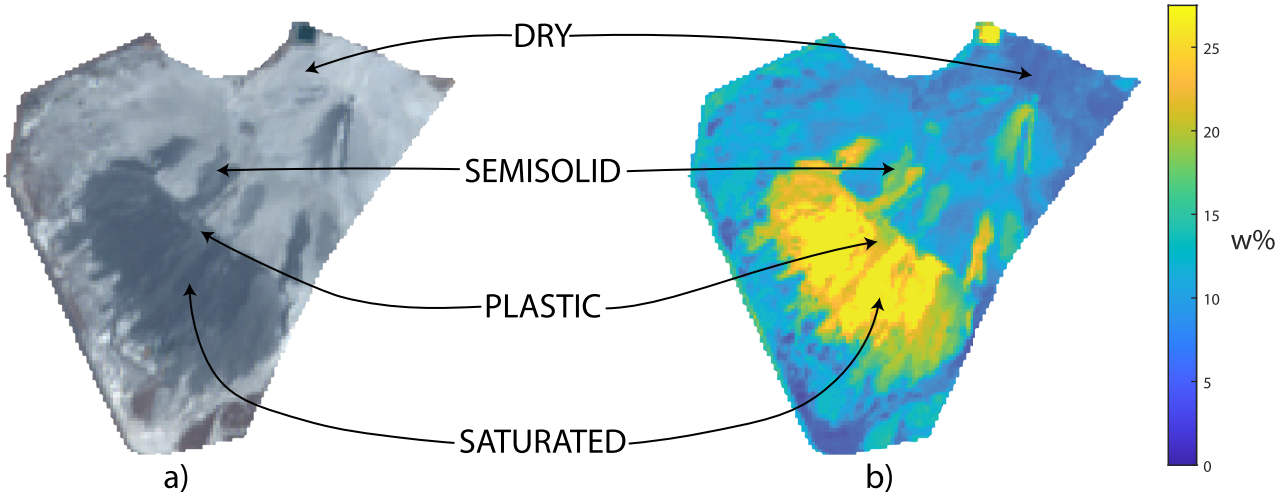

FIGURE 4. a) RGB satellite image captured by Sentinel 2 b) Representation of w% ranges obtained of using methodology [5], [6] [7].

from dry areas (white) to areas of fresh tailings (Dark). Bands (2, 3, and 4) represent the RGB bands that will be used with band 8 (NIR).

At the experimental TTD site, prospecting points were located based on deposition age, dry sectors, fresh tailings and discharge at the time of the fieldwork campaign. Following the same methodology presented in article [5], [6] [7], we obtain the correlations between the images (RGB and NIR) and the in-situ w% of the experimental TTD using the normalized reflection intensity with respect to the dry soil corrected by the spectral power. To exemplify the above, Figure 3a shows an image of light reflection in the satellite NIR band, which includes the 70 surface samples obtained from the experimental TTD and their corresponding normalized reflection curve (Figure 3b), which were used to map values of in-situ w%.

TABLE 1. Field saturation conditions categories and w% rating ranges.

Dry	Semisolid	Plastic	Saturated
0% – 12.8%	12.8% – 17.8%	17.8% – 25.4%	>25.4 %

Once the TTD target outputs are obtained, it is possible to use ML algorithms to perform TTD predictions. Figure 4 shows the RGB image of the TTD and its correspondence to the w% ranges and field saturation conditions categories (Table 1) obtained [8].

IV. METHODOLOGY

The development of our intelligent system we will use ANN, SVM and RF to perform two tasks: **i)** classify the RBG and RGBN image pixels from the experimental TTD into 4 states or categories for thickened tailings (dry, semisolid, plastic, and saturated); **ii)** to estimate (infer) the value of in

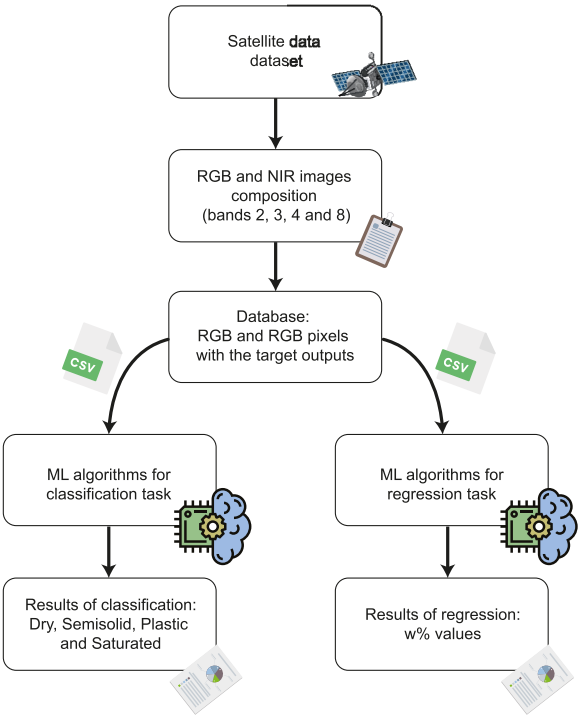

FIGURE 5. Methodology used to estimate w% and classes in TTD using ML algorithms.

situ w% in images of TTD. The methodology to carry out our system is represented in Figure 5. The ML algorithms will be implemented in Keras [36].

A. ARTIFICIAL NEURAL NETWORKS (ANN)

ANN represents a class of models belonging to Deep Learning (subfield of ML) inspired by the behavior of human neurons, and allows systems to learn different tasks, such as prediction and classification of data, detection of objects, natural language processing, among others. Therefore, they are ideal for solving the classification and regression problems analyzed in this document.

The model of a neuron, called the Perceptron, takes inputs x_i, of bias θ_j, with synaptic weights w_{ij}, which represent the learning parameters of the network (see equation 3). The weights are multiplied by their corresponding input, defining the relative importance of each input. The output of the neuron is given by the weighted sum of its inputs, and the following activation function gives flexibility for the ANN to estimate non-linear relationships in the data. Networks with multiple Perceptrons (see Figure 6) – called multilayer networks (MLP) – are used to solve complex problems. ANNs use a backpropagation [35] algorithm to adjust the synaptic weights of the network and thus generate learning. The algorithm operates by obtaining the loss (error) in the output, which is propagated back to the network. In this way, the synaptic weights are updated to minimize the resulting error for each neuron.

B. SUPPORT VECTOR MACHINE (SVM)

The Support Vector Machines (SVM), have presented excellent results when applied in classification with

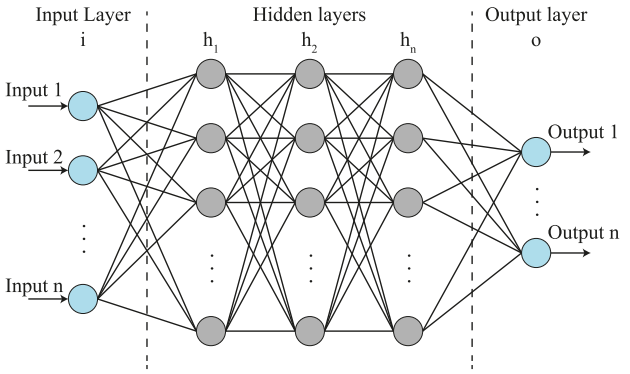

FIGURE 6. Typical representation of an MLP used to generate our system.

traditional techniques. In general, the SVM algorithm seeks to create a hyperplane of separation between two classes.

In the case of SVM, the problem is focused on determining these hyperplanes and establishing the minimum separation margins between classes [37].

One of the most important parameters of the SVMs, is focused on the definition of the kernel, this parameter allows to define the optimization of the definition of separation hyperplanes, especially in the cases of non-linear spaces, within the most known correspond to linear, poly, RBF and sigmoid [38].

As explained in the previous point, the kernel definition plays a fundamental role in the definition of a SVM, there are multiple descriptions for the definition of kernels which allows linear and non-linear searches, the kernel is defined as the representation of the point product, between a pair of data points, in a d-dimensional model the points are represented by $\Phi\left(\overline{X}\right)$, where the kernel function $K\left(\overline{X_i}, \overline{X_j}\right)$ as defined in the equation 2.

$$K\left(\overline{X_i}, \overline{X_j}\right) = \Phi\left(\overline{X_i}\right) \bullet \Phi\left(\overline{X_j}\right) \tag{2}$$

Although the formula previously described in, refers to the generic description for the linear kernel, there are different ways of modeling the similarity between the points, some common choices of the kernel function are shown in Table 2.

Note that SVM for regression purposes is called Support Vector Regression (SVR).

C. RANDOM FOREST (RF)

They are a combination of tree predictors so that each tree depends on the values of an independent random vector with the same distribution for all trees in the forest. The generalization error for forests converges asymptotically to a limit as the forest number becomes large. The generalization error of a forest of tree classifiers depends on the forest's trees' strength and the correlation between them.

Using a random selection of features to split each node yields error rates that compare favorably to Adaboost but are more robust concerning noise. Internal estimates monitor error, strength, and correlation, and these are used to show the response to increasing the number of features used

TABLE 2. Common choice of the kernel functions.

Function	Form
Gaussian radial basis kernel (RBF)	$K\left(\overline{X_i}, \overline{X_j}\right) = e^{\frac{-\left\|\overline{X_i} - \overline{X_j}\right\|^2}{2\sigma^2}}$
Polynomial kernel	$K\left(\overline{X_i}, \overline{X_j}\right) = \left(\overline{X_i} \bullet \overline{X_j} + c\right)^h$
Sigmoid kern	$K\left(\overline{X_i}, \overline{X_j}\right) = tanh\left(\kappa \overline{X_i} \bullet \overline{X_j} - \delta\right)$

in the splitting. Internal assessments are also used to measure variable importance. These ideas are also applicable to regression [39].

$$y_j = f\left(\sum_{i=1}^{N} w_{ij} \cdot x_i + \theta_j\right) \tag{3}$$

V. EXPERIMENTS

The ML algorithms have has two tasks to perform: classification of pixels at different levels into states or categories; and an estimation of w%. Two experiments were performed in order to evaluate the performance of the methods applied to problems of classification of w% ranges and in situ surface states of TTDs.

A. EXPERIMENT 1: CLASSIFICATION OF FIELD SATURATION CONDITIONS FROM W% RANGES

The first experiment aims to classify 4 states or categories of w% of a TTD, representing the following field saturation conditions: dry, semisolid, plastic, and saturated (Table 1).

For our ANN, rectifier type activation functions (ReLU) [40] were used in the hidden layers, with softmax [41] in the output layer. We use a Categorical Cross Entropy loss function [42] and the ADAM optimizer to perform the backpropagation learning. Various configurations and optimizers such as AutoKeras [43] were tested to obtain the parameters of neural networks. The parameters were established 200 epochs at a batch size of 500 and a hidden layer of 160 neurons, which stored only the values of the weights that gave the best results. To avoid overfitting, the Early Stop regularization method [44] was used.

The hyperparameters for SVM and RF was selected using GridSearch, obtaining the best configuration for SVM using C equals to 10, gamma of 0.01 and kernel RBF. For RF we used bootstrap, the depth of each tree in the forest of 4, the number of trees in the forest as 200, the minimum number of samples in a leaf node as 4 for the RGB model and 1 for RGBN model, the minimum number of samples required to split an internal node as 10 for the RGB model and 1 for RGBN model, and we set in auto the number of features to consider when looking for the best split.

i) Training: to train the models, eight images of the experimental TTD at different times (temporal variability) were used. These images totaled 77,536 pixels and each pixel has its respective class. 70% of total available pixels were used, corresponding to the total sum of pixels of the eight selected images.

ii) Validation: the remaining 30% of the original data was used to perform the system validation. This set adjusted model hyperparameters and reviewed existing errors in the model's, such as overfitting the data, and selected the best times and best weights of the neural network model. In this way, a fine adjustment is made to then check the system with test data.

iii) Test: a different set of pixels was used than the ones used in the previous phases. The set has a total of 48,460 pixels from a new set of five images of the TTD obtained over five different dates. This set compares the performance of the model's with data never seen by the classifier.

B. EXPERIMENT 2: ESTIMATION OF IN SITU W%

The second experiment aims to perform the estimation of in situ w% of experimental TTD. Since this is a regression problem, the labels no longer have discrete values (classes). The target value is continuous and represents a specific w% value for one pixel (expressed as a percentage of w%).

The ML models uses the intensity of the pixels of the image of the TTD (RGB or RGBN) as input. For ANN, we use only one neuron, with no activation function, so that the network can generate a number corresponding to the prediction of w%. The training was done through backpropagation. To find the hyperparameters of the network, GridSearch from Sklearn was used. GridSearch evaluated various network models using different combinations of parameters (number of neurons, epochs, optimizers, etc.).

We perform also GridSearch to find the optimal hyperparameter for SVR and RF. Note that exhaustive searching using GridSearch has a high computational cost and significant computation time. The best parameters obtained for SVR are: C equal to 1000, gamma of 0.001 and RBF kernel. In the case of RF we use: number of trees in the forest as 1000 and the minimum number of samples in a leaf node as 3 for the RGB and RGBN model. Once the hyperparameters had been found, a fine-tuning of the model was carried out, looking for the best model performance using the Mean Absolute Error (MAE) metric [45].

i) Training: All images were converted to pixels (RGB and RGBN) with their corresponding labels (w%) to feed the neural network. 70% were selected to perform the training. The ANN uses 125 epochs, with batch size equal to 1 (Stochastic Gradient Descent [46]) and 15 neurons in the hidden layer to perform the training, using parameters obtained from the Gridsearch application.

ii) Validation: The remaining 30% of pixels were used for the validation of the model. We perform an adjustment of the hyperparameters to avoid possible errors and overfitting.

iii) Test: the set had a total of 48,460 pixels from a new set of five images of the TTD obtained over different dates.

TABLE 3. Classification: Comparison of the classification performed by the two models for the same image of TTD in the ML algorithm test.

	Model	Class	Precision	Recall	F1-score	Accuracy
ANN	RGB	Dry	**0.98**	**0.96**	**0.97**	0.93
		Semisolid	0.86	0.80	0.83	
		Plastic	0.82	**0.96**	0.89	
		Saturated	0.92	0.80	0.85	
	RGBN	Dry	0.97	**0.99**	**0.98**	0.95
		Semisolid	0.92	0.88	0.90	
		Plastic	0.92	0.92	0.92	
		Saturated	**0.99**	0.75	0.86	
SVM	RGB	Dry	**0.98**	**0.97**	**0.97**	0.94
		Semisolid	0.88	0.86	0.87	
		Plastic	0.90	0.93	0.91	
		Saturated	0.87	0.85	0.86	
	RGBN	Dry	**0.99**	**0.99**	**0.99**	**0.97**
		Semisolid	0.95	0.95	0.95	
		Plastic	0.96	0.97	0.96	
		Saturated	0.94	0.92	0.93	
RF	RGB	Dry	**0.95**	**0.95**	**0.95**	0.89
		Semisolid	0.79	0.77	0.78	
		Plastic	0.82	0.91	0.86	
		Saturated	0.88	0.51	0.65	
	RGBN	Dry	**0.97**	**0.99**	**0.98**	0.94
		Semisolid	0.90	0.88	0.89	
		Plastic	0.90	0.92	0.91	
		Saturated	0.91	0.60	0.72	

This stage generalized the neural network model adjusted in the training stage and yielded a w% of the tailings dams as unseen data.

VI. RESULTS

A. EXPERIMENTAL RESULTS OF EXPERIMENT 1: CLASSIFICATION OF FIELD SATURATION CONDITIONS FROM W% RANGES

The system was evaluated using the accuracy metric, as is common in ML. In addition, a confusion matrix was used to review the performance obtained in the experiments. These yielded an F1 score and recall [47] to compare results through in-depth analyses. Cross-validation was performed using K-Fold, a robust estimation of the performance of a model with unseen data. For the experiments, K = 10 folds were used.

The results obtained from the ML methods for classification for the test data are shown in Table 3. From the table, it is possible to observe that for ANN, the accuracy obtained is 0.95 for the case of the RGBN model and 0.93 for the model RGB. In both cases, the classification can be carried out correctly, and observing the F1-score metric and recall, the ANN has problems when classifying the saturated class. For SVM, there is a significant increase in accuracy, reaching 0.97 accuracy for the RGBN model and 0.94 for the RGB model. This shows the correct performance of SVM to perform the classification of the 4 classes, due to the use of the RBF kernel that allows searching for non-linear combinations between the data to perform the classification. In addition, this high performance allows each class to be adequately separated from what is observed with the precision values obtained. Regarding RF, the performance shown is the lowest of the 3 ML algorithms, reaching 0.94 for the RGBN model and 0.89 for the RGB model. Note that when using the RGB model, the performances for the ML algorithms are lower than when using the RGBN model, that is, when adding the characteristic of the NIR band, there is a considerable performance increase in the classifiers, reaching a value 0.97 for the SVM case, being our best classification result.

B. EXPERIMENTAL RESULTS OF EXPERIMENT 2: ESTIMATION OF IN SITU W%

In a regression problem, the ML algorithms estimate a numerical value (output) from a series of inputs using the back-propagation algorithm. The distance metrics between the predicted value and the real value are used to analyze the performance of these models. These metrics include the Mean Absolute Error (MAE), the Mean Square Error (MSE) [48], the square root of the Root Mean Square Error (RMSE) and the Mean Absolute Percentage Error (MAPE) [49], which will be used in this experiment. In addition, a 4-Fold was used for this experiment.

The results of the regression experiment for the ML algorithms are presented in Table 4. It is observed that the ANN obtains a good performance for the RGBN model, reaching lower values in all the metrics compared to the RGB model. This effect also occurs in the case of SVR and RF, which indicates that the use of the RGBN model obtains better

TABLE 4. Regression: Comparison of the estimation made by the two models for the same Thickened Tailing Dams image in test for ML algorithms.

	Model	MAE	MSE	RMSE	MAPE	STD	ρ
ANN	RGB	0.67491	1.03931	1.01947	0.05577	0.88820	0.98439
	RGBN	0.37823	0.27215	0.52168	0.03020	**0.33072**	0.99772
SVR	RGB	0.63926	1.17752	1.07384	0.05309	1.08374	0.98323
	RGBN	0.36166	0.28317	0.50483	**0.02943**	0.45656	**0.99776**
RF	RGB	0.70853	1.14711	1.05846	0.05861	1.05986	0.98246
	RGBN	**0.35632**	**0.24559**	**0.47058**	0.02973	0.41775	0.99770

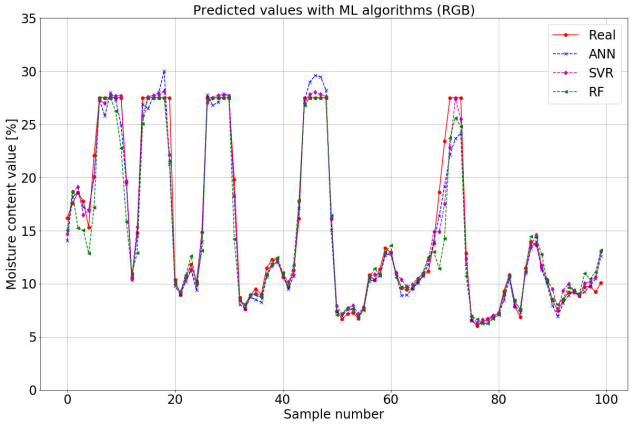

FIGURE 7. Estimation of moisture content for pixels of a TTD using RGB model.

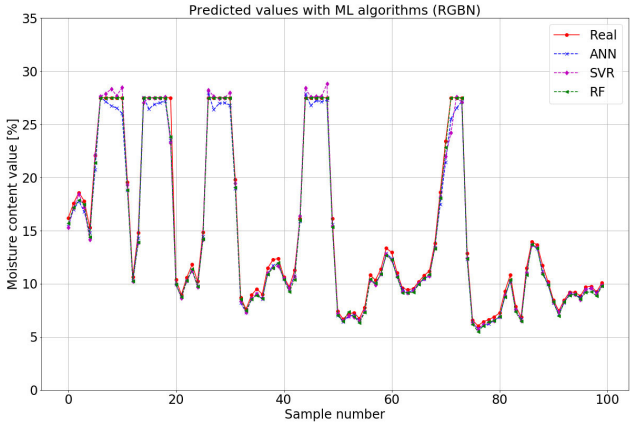

FIGURE 8. Estimation of moisture content for pixels of a TTD using RGBN model.

results than the RGB model, with the NIR characteristic, allowing a better inference of the data. SVR obtains a good performance with MAE values of 0.36 and MAPE of 0.029, which indicates that the model can be used correctly to make predictions of w%. Regarding all the models, the one that achieves the best results according to the metrics used is RF, obtaining an MAE of 0.35, an MSE of 0.24 and an RMSE of 0.47, this implies that this model is the one that should be used to perform the w% forecast.

In relation to the Pearson Correlation Coefficient (ρ) for the RGB and RGBN models, the correlation between the real labels and the predicted labels is clear where, again, the RGBN model shows a higher result than the RGB model, showing a clear contribution from the infrared channel (NIR).

Again, the use of an extra feature greatly improves the results for the test set. The results of the metrics are clearly reflected in the graphs of the predictions shown below (Table 4). Figure 7 shows the predictions of the w% values when using the RGB model. It is observed that for w% below 15%, the estimation error of the network is low, approaching real values. However, there is a significant increase in error when estimating higher w% values. The situation improves when incorporating the infrared channel, since for the RGBN model (Figure 8), the estimation error decreases drastically, having reliable estimates, even for w% values close to the saturation zone (w% > 25.4%).

In the case of the ANN, there is an increment in the error when estimating high w%, however, in the case of SVR and RF, the error is low, adapting better to the high changes in w%. Note the good performance of RF, adjusting the forecast correctly.

VII. DISCUSSION

Experiment 1 showed that the RGBN model obtained slightly improved performance in terms of accuracy in comparison to the RGB model. Tables 3 and 4 show that the RGBN model outperforms the RGB model across every metric. We can conclude from this that the NIR band introduces new information to the model, thus obtaining better performance. Also, if we compare the results across the 4 classes, we observe that field saturation conditions categories (Dry, Semisolid and Plastic) obtained obtained high recall, with the exception of the Saturated class, with slightly worse results. However, one may infer that this is the most difficult class to classify correctly due to the low number of examples available for training this class.

Experiment 2 showed similar model outcomes for the addition of the NIR band. The results of the RGBN model outperform those of the RGB model in every performance measure: comparing Figures 7 and 8 shows that the inclusion of the NIR band allows the model to make better predictions in the peaks of the curve, especially for RF case.

VIII. CONCLUSION

This work has demonstrated an approach for accurately modelling field saturation condition categories (Dry, Semisolid, Plastic and Saturated) using ML algorithms based on remote sensing images.

The proposed methodology constitutes a tool for periodically monitoring surface w% of thickened tailings layers over time, and is much more practical and precise than current on-site visual inspection operators.

This is a key contribution to ensuring geotechnical control variables for the operation and physical stability of TTDs, particularly in countries with high seismic activity and projected tailings productions, such as in Chile. Indeed, this research directly addresses the national tailings policy, established in the 2015-2035 Technological Roadmap, whose strategic priority is the development of a technological program for monitoring tailings deposits, specifically: generating models that can be updated online to establish a stability index; developing online instrumentation for monitoring; providing physicochemical measurements of the infiltrations produced since the operation of the tailings dams; and developing networks, protocols, and systems to share the information with communities.

Future work will continue to expand upon new deep learning techniques to better estimate labels. The application of ML to TTD management constitutes an interesting alternative for integrating data across operational monitoring, and thus improve resolution on the understanding of physical stability, both in the short, operational term, and the long, closure term.

REFERENCES

[1] *Mineral Commodity Summaries 2020*, U.S. Geol. Surv., Reston, VA, USA, 2020.

[2] *Proyección de la Producción de Cobre En Chile 2018–2029*, Comisión Chilena del Cobre, Santiago, Chile, 2019.

[3] SERNAGEOMIN, Santiago, Chile. *Datos Públicos Depósito de Relaves. Catastro de Depósitos de Relaves en Chile*. Accessed: Sep. 3, 2020, [Online]. Available: https://www.sernageomin.cl/datos-publicos-deposito-de-relaves/

[4] G. Villavicencio, R. Espinace, J. Palma, A. Fourie, and P. Valenzuela, "Failures of sand tailings dams in a highly seismic country," *Can. Geotech. J.*, vol. 51, no. 4, pp. 449–464, Apr. 2014, doi: 10.1139/cgj-2013-0142.

[5] V. Araya, G. Suazo, G. Villavicencio, and M. Silva, "Monitoreo de la Humedad en depósitos de relave a partir de mediciones de reflexión de luz," *Obras y Proyectos*, no. 25, pp. 35–41, 2019, doi: 10.4067/S0718-28132019000100035.

[6] V. Araya, G. Suazo, G. Villavicencio, and M. Silva, "Use of UAV and satellite images for the monitoring of water content in tailings storage facilities," presented at the Conf. Paste, Santiago, Chile, Jul. 2018.

[7] M. Sanchez, V. Araya, and G. Suazo, "Monitoring of moisture content in paste tailings using hyperspectral cameras," presented at the 23rd Int. Conf. Paste, Thickened Filtered Tailings. Santiago, Chile: Gecamin, 2020, doi: 10.36487/ACG_repo/2052_105.

[8] R. Espinace, G. Villavicencio, and J. C. Torrejon, "Últimos avances en el control operacional de los depósitos de relave con la tecnología Panda. Aplicación en Chile," presented at the 10th Chilean Congr. Geotech. Eng., Valdivia, Chile, Dec. 2016.

[9] R. Verdugo, "Seismic performance based-design of large earth and tailing dams," in *Performance-Based Design in Earthquake Geotechnical Engineering*, 1st ed. London, U.K: CRC Press, 2009, pp. 41–60.

[10] A. G. Villavicencio, P. Breul, C. Bacconnet, D. Boissier, and A. R. Espinace, "Estimation of the variability of tailings dams properties in order to perform probabilistic assessment," *Geotech. Geol. Eng.*, vol. 29, no. 6, pp. 1073–1084, Nov. 2011, doi: 10.1007/s10706-011-9438-5.

[11] J. M. Pereira, "Big data et intelligence artificielle en géotechnique: Où en est-on ? Où va-t-on?" in *Proc. Solscope*, Marseille, France, Jun. 2019, pp. 1–7.

[12] P. Pirnia, F. Duhaime, and M. Manashti, "Machine learning algorithms for applications in geotechnical engineering," in *Proc. GeoEdmonton*, Edmonton, AB, Canada, 2018, pp. 1–37.

[13] N. Puri, H. D. Prasad, and A. Jain, "Prediction of geotechnical parameters using machine learning techniques," in *Proc. 6th Int. Conf. Smart Comput. Commun. (ICSCC)*, Kurukshetra, India, vol. 125, Dec. 2017, pp. 509–517, doi: 10.1016/j.procs.2017.12.066.

[14] R. Espinace, G. Villavicencio, and A. Fourie, "Importance of geotechnical operational control of thickened tailings deposits," presented at the Conf. Paste, Santiago, Chile, Jul. 2016.

[15] G. Barrios, E. Sáez, and C. Ledezma, "Influence of desiccation cracking on the liquefaction potential of thickened tailing deposits," in *Proc. 15WCEE*, Lisboa, Portugal, Sep. 2012, pp. 14992–15033.

[16] *Tailings Deposits—Control of Compaction With Light Dynamic Penetrometer*. Nch 3261-12, INN, Santiago, Chile, 2012.

[17] L. Weidong, F. Baret, G. U. Xingfa, T. Qingxi, Z. Lanfen, and Z. Bing, "Relating soil surface moisture to reflectance," *Remote Sens. Environ.*, vol. 81, nos. 2–3, pp. 238–246, 2002, doi: 10.1016/S0034-4257(01)00347-9.

[18] L. Hassan-Esfahani, A. Torres-Rua, A. Jensen, and M. McKee, "Assessment of surface soil moisture using high-resolution multi-spectral imagery and artificial neural networks," *Remote Sens.*, vol. 7, no. 3, pp. 2627–2646, Mar. 2015, doi: 10.3390/rs70302627.

[19] E. Taktikou, G. Bourazanis, G. Papaioannou, and P. Kerkides, "Prediction of soil moisture from remote sensing data," in *Proc. Int. Conf. Efficient Sustain. Water Syst. Manage. Toward Worth Living Develop., 2nd EWaS*, vol. 162, 2016, pp. 309–316, doi: 10.1016/j.proeng.2016.11.066.

[20] M. Sadeghi, S. Jones, and M. Tuller, "Toward a calibration-free model for optical remote sensing of soil moisture," presented at the Conf., AGU Fall Meeting, San Francisco, CA, USA, Dec. 2015.

[21] M. Sadeghi, E. Babaeian, M. Tuller, and S. B. Jones, "Particle size effects on soil reflectance explained by an analytical radiative transfer model," *Remote Sens. Environ.*, vol. 210, pp. 375–386, Jun. 2018, doi: 10.1016/j.rse.2018.03.028.

[22] I. Entezari, B. Rivard, M. Lipsett, and W. Wilson, "Application of hyperspectral remote sensing in estimation of oilsands tailings water content," in *Proc. 5th Workshop Hyperspectral Image Signal Process., Evol. Remote Sens. (WHISPERS)*, Gainesville, FL, USA, Jun. 2013, pp. 1–4.

[23] M. A. Shahin, M. B. Jaksa, and H. R. Maier, "State of the art of artificial neural networks in geotechnical engineering," *Electron. J. Geotech. Eng.*, vol. 8, no. 1, pp. 1–26, 2008.

[24] A. Elshorbagy, G. Corzo, S. Srinivasulu, and D. P. Solomatine, "Experimental investigation of the predictive capabilities of data driven modeling techniques in hydrology—Part 1: Concepts and methodology," *Hydrol. Earth Syst. Sci.*, vol. 14, no. 10, pp. 1931–1941, Oct. 2010, doi: 10.5194/hess-14-1931-2010.

[25] N. S. Juwaied, "Applications of artificial intelligence in geotechnical engineering," *J. Eng. Appl. Sci.*, vol. 13, no. 8, pp. 2764–2785, 2018.

[26] M. J. Sulewska, "Applying Artificial Neural Networks for analysis of geotechnical problems," *Comput. Method. Appl. Eng. Sci.*, vol. 18, no. 4, pp. 231–241, 2011.

[27] L. Dong, W. Shu, D. Sun, X. Li, and L. Zhang, "Pre-alarm system based on real-time monitoring and numerical simulation using Internet of Things and cloud computing for tailings dam in mines," *IEEE Access*, vol. 5, pp. 21080–21089, 2017, doi: 10.1109/ACCESS.2017.2753379.

[28] R. Balaniuk, O. Isupova, and S. Reece, "Mining and tailings dam detection in satellite imagery using deep learning," 2020, *arXiv:2007.01076*. [Online]. Available: http://arxiv.org/abs/2007.01076

[29] D. Hong, L. Gao, J. Yao, B. Zhang, A. Plaza, and J. Chanussot, "Graph convolutional networks for hyperspectral image classification," *IEEE Trans. Geosci. Remote Sens.*, early access, Aug. 18, 2020, doi: 10.1109/TGRS.2020.3015157.

[30] E. Ferreira, M. Brito, R. Balaniuk, M. S. Alvim, and J. A. D. Santos, "BrazilDAM: A benchmark dataset for tailings dam detection," 2020, *arXiv:2003.07948*. [Online]. Available: http://arxiv.org/abs/2003.07948

[31] F. Nasategay, "Detection and monitoring of tailings dam surface erosion using UAV and machine learning," M.S. thesis, Mining Eng., Univ. Nevada, Reno, NV, USA, 2020.

[32] N. Baghdadi, R. Cresson, M. E. Hajj, R. Ludwig, and I. La Jeunesse, "Estimation of soil parameters over bare agriculture areas from C-band polarimetric SAR data using neural networks," *Hydrol. Earth Syst. Sci.*, vol. 16, no. 6, pp. 1607–1621, Jun. 2012.

[33] C. Xing, N. Chen, X. Zhang, and J. Gong, "A machine learning based reconstruction method for satellite remote sensing of soil moisture images with *in situ* observations," *Remote Sens.*, vol. 9, no. 5, p. 484, May 2017.

[34] Y. Liu, Y. Yang, W. Jing, and X. Yue, "Comparison of different machine learning approaches for monthly satellite-based soil moisture downscaling over Northeast China," *Remote Sens.*, vol. 10, no. 2, p. 31, Dec. 2017.

[35] D. E. Rumelhart, G. E. Hinton, and R. J. Williams, "Learning representations by back-propagating errors," *Nature*, vol. 323, no. 6088, pp. 533–536, Oct. 1986, doi: 10.1038/323533a0.

[36] J. Moolayil, "An introduction to deep learning and Keras," in *Learn Keras for Deep Neural Networks*. Vancouver, BC, Canada: Apress, 2019, pp. 1–16.
[37] C. Aggarwal, *Machine Learning for Text*. Cham, Switzerland: Springer, 2018, doi: 10.1007/978-3-319-73531-3.
[38] F. Pedregosa, G. Varoquaux, A. Gramfort, V. Michel, B. Thirion, O. Grisel, M. Blondel, P. Prettenhofer, R. Weiss, V. Dubourg, J. Vanderplas, A. Passos, D. Cournapeau, M. Brucher, M. Perrot, and E. Duchesnay, "Scikit-learn: Machine learning in Python," *J. Mach. Learn. Res.*, vol. 12, pp. 2825–2830, 2011. Accessed: Dec. 31, 2020. [Online]. Available: https://scikit-learn.org/stable/modules/svm.html#svm/
[39] L. Breiman, "Random Forests," *Mach. Learn.*, vol. 45, no. 1, pp. 5–32, 2001, doi: 10.1023/A:1010933404324.
[40] A. F. Agarap, "Deep learning using rectified linear units (ReLU)," 2018, *arXiv:1803.08375*. [Online]. Available: http://arxiv.org/abs/1803.08375
[41] S. Gold and A. Rangarajan, "Softmax to softassign: Neural network algorithms for combinatorial optimization," *J. Artif. Neural*, vol. 2, no. 4, pp. 381–399, 1996.
[42] F. Farahnak-Ghazani and M. S. Baghshah, "Multi-label classification with feature-aware implicit encoding and generalized cross-entropy loss," in *Proc. 24th Iranian Conf. Electr. Eng. (ICEE)*, Shiraz, Iran, May 2016, pp. 1574–1579.
[43] H. Jin, Q. Song, and X. Hu, "Auto-keras: An efficient neural architecture search system," in *Proc. 25th ACM SIGKDD Int. Conf. Knowl. Discovery Data Mining*, Anchorage, AK, USA, Jul. 2019, pp. 1946–1956.
[44] L. Prechelt, "Early stopping-but when?" in *Neural Networks: Tricks of the Trade* (Lecture Notes in Computer Science), vol. 1524, G. B. Orr and K. R. Müller, Eds. Berlin, Germany: Springer, 1998, pp. 55–69, doi: 10.1007/3-540-49430-8_3.
[45] C. Willmott and K. Matsuura, "Advantages of the mean absolute error (MAE) over the root mean square error (RMSE) in assessing average model performance," *Climate Res.*, vol. 30, no. 1, pp. 79–82, 2005, doi: 10.3354/cr030079.
[46] S. Ruder, "An overview of gradient descent optimization algorithms," 2016, *arXiv:1609.04747*. [Online]. Available: http://arxiv.org/abs/1609.04747
[47] C. Goutte and E. Gaussier, "A probabilistic interpretation of precision, recall and F-score, with implication for evaluation," in *Advances in Information Retrieval*. Berlin, Germany: Springer, 2005, pp. 345–359.
[48] J. N. K. Rao, J. Jiang, and K. Das, "Mean squared error of empirical predictor," *Ann. Statist.*, vol. 32, no. 2, pp. 818–840, Apr. 2004, doi: 10.1214/009053604000000201.
[49] A. D. Myttenaere, B. Golden, B. L. Grand, and F. Rossi, "Mean absolute percentage error for regression models," *Neurocomputing*, vol. 192, pp. 38–48, Jun. 2016, doi: 10.1016/j.neucom.2015.12.114.

GABRIEL VILLAVICENCIO ARANCIBIA was born in Valparaíso, Chile, in 1977. He received the Ph.D. degree in civil engineering from the Ecole Doctorale des Sciences pour l'Ingénieur. Université Blaise Pascal, Clermont II, France, in 2009. From 2004 to 2009, he was a temporary teaching and research associates with the Civil Engineering Department, Polytech Clermont-Ferrand, France. Since 2010, he has been an Assistant Professor with the Construction Engineering of the Pontificia Universidad Católica de Valparaíso, and Geotechnical Engineer with the LEPUCV Laboratory. His research interests include geotechnical engineering applications for tailings dams, wasted rocks dumps, and heap leach pad. In addition, in topics such as evaluation of liquefaction potential, slope stability, and geotechnical modeling of urban sites. He is an active member of the Geotechnics Group PUCV and of the Chilean Geotechnical Society.

OSVALDO PIÑA BUSTAMANTE was born in Santiago, Chile, in 1987. He received the degree in electronic engineering from the Pontificia Universidad Católica de Valparaíso, Chile, in 2019. Since 2018, he has worked as a Collaborator in projects focused mainly on computer vision applying AI algorithms. His research interests include image processing, object recognition, people recognition, and computer vision.

GABRIEL HERMOSILLA VIGNEAU was born in Chillan, Chile, in 1982. He received the degree in electronic engineering from the University of La Frontera, Temuco, Chile, in 2007, and the Ph.D. degree in electric engineering from the University of Chile, Santiago, Chile, in 2012. Actually, he is an Associate Professor with the School of Electrical Engineering, Pontificia Universidad Católica de Valparaiso (PUCV), Valparaiso, Chile. His main areas of research interest are thermal face recognition, pattern recognition, computer vision, and deep learning.

HÉCTOR ALLENDE-CID was born in Valparaíso, Chile, in 1983. He received the Ph.D. degree from Universidad Técnica Federico Santa María, Chile, in 2015. He is currently an Assistant Professor with the Escuela de Ingeniería Informática, Pontificia Universidad Católica de Valparaíso. His research interests include supervised algorithms, distributed machine learning methods, and natural language processing.

GONZALO SUAZO FUENTELABA was born in Chile in 1983. He received the Ph.D. degree in geotechnical engineering from The University of Western Australia, Australia, in 2015. Since 2015, he has been working as an Assistant Professor with the Civil Engineering Department at Universidad Técnica Federico Santa Maria, Chile. He has also been involved as a geotechnical engineer in several large projects related to tailings management in Chile, Perú, and Australia. He expertise is in laboratory and in situ characterization of the monotonic and seismic response of tailings materials and other mining byproducts. He is an active member of ICOLD and the Chilean Society of Geotechnical Engineering.

VICTOR ARAYA NIETO was born in Chile in 1991. He received the M.Sc. degree in civil engineering from The Universidad Técnica Federico Santa Maria, Chile, in 2017. Since 2017, he has been working as a Researcher with the Civil Engineering Department, Universidad Técnica Federico Santa Maria, Chile. His research interests include geophysics, remote sensing, and image processing. He has been working on the development of laboratory and field instrument to monitoring tailings storage facilities.